"Water-in-Salt" Electrolyte Makes Aqueous Sodium-Ion Battery Safe, Green, and Long-Lasting

Liumin Suo, Oleg Borodin, Yuesheng Wang, Xiaohui Rong, Wei Sun, Xiiulin Fan, Shuyin Xu, Marshall A. Schroeder, Arthur V. Cresce, Fei Wang, Chongyin Yang, Yong-Sheng Hu, Kang Xu,* and Chunsheng Wang**

Narrow electrochemical stability window (1.23 V) of aqueous electrolytes is always considered the key obstacle preventing aqueous sodium-ion chemistry of practical energy density and cycle life. The sodium-ion water-in-salt electrolyte (NaWiSE) eliminates this barrier by offering a 2.5 V window through suppressing hydrogen evolution on anode with the formation of a Na^+-conducting solid-electrolyte interphase (SEI) and reducing the overall electrochemical activity of water on cathode. A full aqueous Na-ion battery constructed on $Na_{0.66}[Mn_{0.66}Ti_{0.34}]O_2$ as cathode and $NaTi_2(PO_4)_3$ as anode exhibits superior performance at both low and high rates, as exemplified by extraordinarily high Coulombic efficiency (>99.2%) at a low rate (0.2 C) for >350 cycles, and excellent cycling stability with negligible capacity losses (0.006% per cycle) at a high rate (1 C) for >1200 cycles. Molecular modeling reveals some key differences between Li-ion and Na-ion WiSE, and identifies a more pronounced ion aggregation with frequent contacts between the sodium cation and fluorine of anion in the latter as one main factor responsible for the formation of a dense SEI at lower salt concentration than its Li cousin.

1. Introduction

Lithium-ion batteries (LIBs) have successfully changed our lives, but its adoption by larger-format applications (10^3–10^6 W h) like vehicle electrification and grid-storage inevitably encounters the availability issue of lithium as a natural source, along with potential safety and environmental risks brought by the inflammable and toxic nonaqueous electrolytes. In contrast, sodium (Na) is highly abundant and readily accessible in both earth-crust and ocean. An aqueous Na-ion batteries would be far more economically competitive than LIBs for large-format applications, where cost, safety, greenness, and cycle-life outweigh energy density considerations,[1] and would provide an ideal resolution to all these concerns mentioned above.[2–4]

Historically, aqueous electrolytes have been known for their narrow electrochemical stability window (<1.50 V), as defined by the decomposition reaction of water,[5,6] which imposes an unwanted restriction on the choice of electrochemical couples (cathode and anode materials) and consequently the practical energy output of such aqueous battery chemistries.[7] Only those anode materials that operate at relatively high potentials have been used for aqueous Na-ion batteries, such as $NaTi_2(PO_4)_3$ (2.1 V vs Na),[3,8] Prussian blue analogues,[4] vanadium oxide including $V_2O_5 \cdot 0.6H_2O$[9] and $Na_2V_6O_{16} \cdot nH_2O$,[10] or organic anodes including disodium naphthalenediimide (SNDI) (2.57 V vs Na),[11] polyimide anode,[12] and PPy-coated MoO_3 (2.3–2.4 V vs Na).[13] Among these, $NaTi_2(PO_4)_3$ with NASICON structure has a long cycling stability, and hence has been extensively investigated. However, since this potential (2.10 V vs Na) is slightly lower than hydrogen evolution potential (2.297 V vs Na), water decomposition still inevitably occurs in aqueous Na-ion battery constructed with $NaTi_2(PO_4)_3$ anode. Such irreversible process not only builds up internal pressure due to hydrogen evolution but also depletes Na from the cathode, which is a limited source in a full Na-ion cell. In a similar manner, the operation potential of the most commonly used cathode material for sodium intercalation, $Na_{0.66}[Mn_{0.66}Ti_{0.34}]O_2$, also situates slightly beyond the anodic stability limit of aqueous electrolyte, where O_2 is produced during repeated charge/discharge cycles. Consequently, such aqueous Na-ion batteries are characterized by steady capacity losses as well as low Coulombic efficiencies. In previous reports, high cycling rates were often adopted so that impressive cycle numbers could be accumulated before the effect of water decomposition on cycle life becomes visible.

Dr. L. Suo, W. Sun, Dr. X. Fan, Dr. F. Wang, Dr. C. Yang, Prof. C. Wang
Department of Chemical and Biomolecular Engineering
University of Maryland College Park
MD 20740, USA
E-mail: cswang@umd.edu

Dr. O. Borodin, Dr. M. A. Schroeder, Dr. A. V. Cresce, Dr. K. Xu
Electrochemistry Branch, Sensor and Electron Devices Directorate
Power and Energy Division U.S. Army Research Laboratory Adelphi
MD 20783, USA
E-mail: conrad.k.xu.civ@mail.mil

Dr. Y. Wang, X. Rong, Dr. S. Xu, Prof. Y.-S. Hu
Key Laboratory for Renewable Energy
Beijing Key Laboratory for New Energy Materials and Devices
Beijing National Laboratory for Condensed Matter Physics
Institute of Physics
Chinese Academy of Sciences
School of Physical Sciences
University of Chinese Academy of Sciences
Beijing 100190, China
E-mail: yshu@iphy.ac.cn

DOI: 10.1002/aenm.201701189

Apparently, this tactical measure is impractical and nonsustainable for actual applications such as grid storage, where cells will have to be charged at low rates, and capacity has to be retained at charged states upon prolonged standings.

In this work, we applied "water-in-salt" concept to expand the stability window of Na-ion aqueous electrolyte, in the hope that similar kinetic protection effect as observed in the Li version of "water-in-salt" electrolyte (LiWiSE) would occur. Solid-electrolyte interphase (SEI) has been best known for such kinetic protection in LIBs that uses nonaqueous electrolytes based on carbonate solvents. Recently, we reported that an aqueous SEI is possible as long as Li^+-solvation sheath is sufficiently populated by proper anions.[14] Here, we show for the first time that a Na version of WiSE (NaWiSE) based on sodium trifluoromethane sulfonate ($NaCF_3SO_3$, or NaOTF) can indeed form a Na^+-conducting SEI on $NaTi_2(PO_4)_3$ anode surface and effectively suppress hydrogen evolution. Meanwhile, the reduced electrochemical activity of water also leads to hindered oxygen evolution on $Na_{0.66}[Mn_{0.66}Ti_{0.34}]O_2$ cathode. An overall electrochemical stability window of 2.5 V is thus usable for Na-ion chemistries. Such expanded window allows a full Na-ion battery constructed on $Na_{0.66}[Mn_{0.66}Ti_{0.34}]O_2$ and $NaTi_2(PO_4)_3$ to function with unprecedented reversibility, as evidenced by extraordinarily high Coulombic efficiency (>99.2%) even at a low rate of 0.2 C for >350 cycles. At a high rate of 1 C, superior long-term cycle life of >1200 cycles was also achieved, with negligible capacity losses (0.006% per cycle). We believe that these encouraging performances enlighten a new direction for the development of practical aqueous Na-ion battery of excellent cycle-life, ultimate safety as well as environmental friendliness.

2. Results and Discussion

As the universal solvent on this planet, water molecule is highly polar with a high dielectric constant (78.3 at room temperature). The lone electron pair on its oxygen serves as strong Lewis base to coordinate with cations, while hydrogen as strong Lewis acid for anions. These characteristics provide water molecule with such strong solvation power toward most salts that the dissociated ions are often trapped in "solvation cages" formed by O or H atoms. Cations in particular are more tightly bound by water molecules than anions due to their smaller sizes and much stronger Coulombic attraction to Lewis base than do anions.[15] For Na^+ in dilute aqueous solutions below 5 M, where water molecules far outnumber the salt, it is generally accepted that its solvation sheath consists of at least two layers: the more-tightly associated primary and the relatively loose secondary solvation shell (**Figure 1**a), with the first Na^+ solvation shell typically containing 6 oxygens.[16] However, when salt concentration is above 9.00 M, there are barely enough water molecules available to form the "classical" primary solvation sheath, and the resultant "water-in-salt" solution can then be visualized as a liquefied salt. As reported recently, a series of new properties including that of both transport and interphasial chemistry become possible in the realm of such highly concentrated solutions.

It has been shown previously that, in the Lithium bis(trifuoromethanesulfonyl)imide (LiTFSI)–H_2O system, the Li salt was largely dissociated when there were more than 6–10 water molecules per Li^+. In order to induce widespread aggregation and eliminate free water, so that the desired aqueous protective interphase-formation could be realized, the water/cation ratio must be lower than 3.[14] Interestingly, aggregation behavior differs significantly in the NaOTF–H_2O system, granting us the desired interphasial benefits at much lower salt concentrations. Figure 1b and Figure S1 (Supporting Information) show the salt aggregation in NaOTF–H_2O as probed via Raman spectroscopy, in which the evolution of the SO_3 stretching band with salt concentration was examined. From 2 to 9.26 M, the overall peak (black solid line in Figure 1b) experiences a blueshift. Its deconvolution in 9.26 M reveals two major bands, attributed, respectively, to the solvent-separated ion pairs (SSIP, Na–$(H_2O)_n$–OTF: 1032 cm^{-1}) and contact ion pairs (CIP, NaOTF)/aggregated cation–anion pairs (AGG, $Na_nCF_3SO_3)^{(n-1)+}$, 1040 cm^{-1}) (Table 1 and Figure 1d). The evolution of this band indicated that the SSIPs fraction dramatically drops below 70% at only 6 M salt concentration, or <40% at 9.26 M, where majority of salt species already exist as CIP/AGG at high salt concentrations than its Li cousin (Figure 1b and Table 1). A density-function theory (DFT) analysis of the changes in this band upon Na^+ complexation reveals a strong dependence of the band shift on the Na^+ position relative to SO_3-group of the anion, which complicates Raman spectrum interpretation as discussed in supporting information (Figures S2–S5, Supporting Information). However, when the position-dependent shifts of the $\nu_s(SO_3)$ band calculated from DFT are combined with the probability of finding the Na^+ cation in these positions from molecular dynamics (MD) simulations, the distribution of $\nu_s(SO_3)$ shifts was obtained (Figure 1c). The most probable blue-shift of 8 cm^{-1} for the $\nu_s(SO_3)$ band of CIP compared to SSIP and the shape of the shift curve obtained from modeling agree excellently with the Raman decomposition results, which support our band assignment (Figure 1b) and strongly suggests that the majority of ions at 9.26 M were indeed part of ion pairs or aggregates. MD simulations using a many-body polarizable force field were also utilized to examine ion aggregation and transport. The excellent agreement between the predicted and experimental values of ionic conductivity further validates the simulation model (Figure S6, Supporting Information). Overall, a significant degree of ion pairing and aggregation were found in all three simulated concentrations of the NaOTF–H_2O: 4, 6, and 9.3 M at 60 °C, yielding 0.66, 1.16, and 1.7 anions coordinating a Na^+ on average, in a sharp contrast with the LiTFSI–H_2O electrolyte. Moreover, when an immediate (or compact) solvation shell (R(S(anion)–Na^+) < 3.7 Å) of anion was examined at 9.3 m salt concentration, MD simulations predicted that 30% of ions exist as solvent-separated ion in good agreement with Raman data. When considering the full solvation shell R(S(anion)-Na^+) < 4.4 Å), only 14% of anions would be solvent-separated from Na^+, indicating that the most anions are in the close vicinity of Na^+, and would likely participate in interphasial chemistry during Na^+-intercalation into anode host discussed below.

In order to provide further support for CIP and aggregate existence in NaOTF–H_2O system, relative free energies of the SSIP and CIP were also calculated using quantum chemistry (QC) calculations through a cluster–continuum approach, in

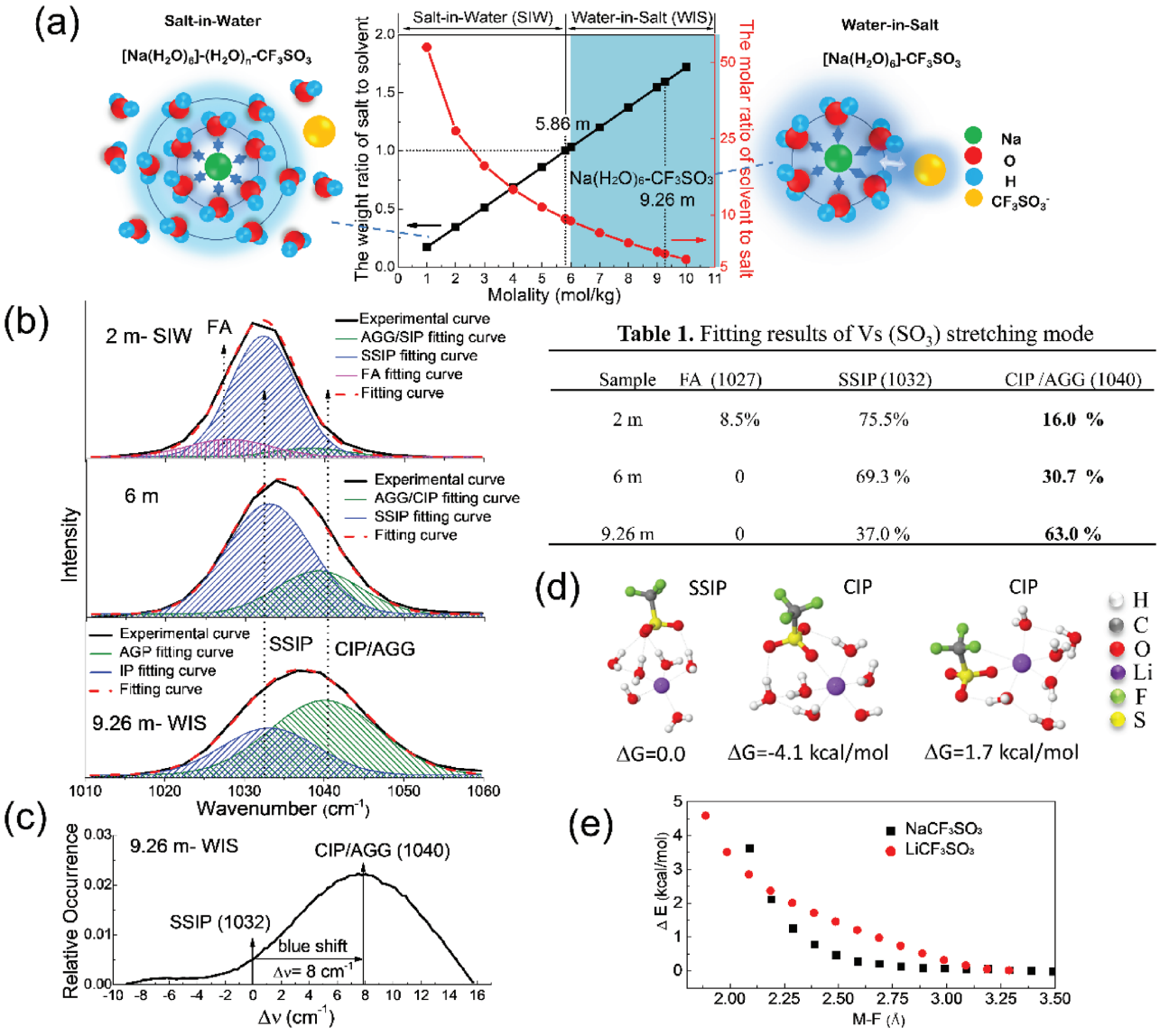

Table 1. Fitting results of Vs (SO_3) stretching mode

Sample	FA (1027)	SSIP (1032)	CIP /AGG (1040)
2 m	8.5%	75.5%	**16.0 %**
6 m	0	69.3 %	**30.7 %**
9.26 m	0	37.0 %	**63.0 %**

Figure 1. The cation–anion and ion–solvent interactions in NaWiSE. a) The molar and weight salt/solvent ratios in NaOTF–H_2O binary system, whose corresponding temperature dependences of ion conductivities is shown in Figure S6 (Supporting Information). b) SO_3 stretching mode in Raman spectra for electrolytes of different salt concentrations (2, 6, and 9.26 m), c) relative occurrence of anion ν_s (SO_3) band shift versus isolated OTF^- anion obtained from molecular modeling by combining the frequency shifts from DFT calculations shown in Figure S4 (Supporting Information) and probability distribution for the S=O···Na angle extracted from MD simulations, d) relative free energies at 298 K of CIP versus SSIP from G4MP2 QC calculations using SMD (water) implicit solvent model, and e) energy profiles for the Li^+ and Na^+ cation to approach fluorine of OTF-anion from M06-L/6-31+(d,p) DFT calculations with SMD (water) implicit solvation model. Table 1 lists the anion complex proportion of free anion (FA), the solvent separated ion pairs (SSIP), and contact ion pairs (CIP) or Aggregation (AGG) based on the fitting results of ν_s (SO_3) stretching mode from (a). **Table 1**. Fitting results of Vs (SO_3) stretching mode of Figure 1b.

which 6 water molecules in the immediate anion solvation shell were included explicitly as shown in Figure 1d, while water beyond it was modeled as implicit solvent. The CIPs were found to have slightly lower free energies than SSIP, suggesting that contact ion pair formation might prevail even at low to moderate concentrations. The structure with the Na^+ coordinated by both F and O in OTF-anion was found to be only 1.7 kcal mol^{-1} less stable than SSIP indicating that such structures, while not dominant, are expected to be present in solution. Indeed, as Figure 1e shows, Na^+ is able to approach the F without significant energetic penalty. Interestingly, a much higher energy penalty for the Li–F approach was observed in the Li analog for metal-fluoride distances >2.2 Å. This fundamental difference in NaWiSE and LiWiSE constitutes the basis of forming a dense Na^+-conducting interphase at relatively low salt concentration because of the viability of the F-abstraction and NaF formation as a result of reduction of the cation–anion aggregates.

As expected, the intensified cation–anion association results in decreasing ion conductivities from the diluted states

(Figure S6, Supporting Information). Nevertheless, at 9.26 m, the conductivity (50 mS cm^{-1}) still maintains a high value, being five times higher than what typical nonaqueous electrolytes can offer (10 mS cm^{-1}).[17] Moreover, MD simulations predict more than 40% faster diffusion of cation compared to anion at this concentration at 333 K, suggesting high cation transference number. According to Yamada et al.,[18] a superionic region should exist at such high salt concentrations as result of the disruption of water network that normally exists in diluted aqueous solutions. The high ionic population occupying the coordination capability of both O and H breaks the hydrogen bonding between water molecules while making the solvent matrix less viscous than what Walden's rule would predict. As a result, ion conduction decouples from the solvent cages.

While ion aggregation reduces ionic conductivity, it is beneficial for the formation of an aqueous interphase that stabilizes water molecules against the reducing surfaces of the anode materials.[14,19] Similar to what found in LiWiSE, high salt aggregation and intimate Na–F contacts present in NaWiSE help in raising salt reduction potential above that of hydrogen evolution. **Figure 2**a shows the calculated salt reduction potentials for various configurations spanning from CIP to aggregates. Reduction of CIPs or aggregates without NaF formation occurs at potentials slightly lower than 2.0 V versus Na/Na^+, while reduction of the $NaCF_3SO_3$ aggregates resulting in NaF formation occurs above 2.4 V versus Na/Na^+, i.e., before the decomposition of water molecule (2.29 V), thus granting an opportunity for the anode being protected by NaF during the first charging cycle. What differs from the reported LiWiSE is that the salt concentration required for such interphase formation in NaWiSE (≈9.0 m) is far below what required for LiTFSI (21 m). The further details of MD and DFT calculation about the mechanism of anion reduction, ion aggregation, and Li ionic transportation in different concentrated electrolytes are presented in SI (Figures S7–S11, Supporting Information).

Compared with the LiF-rich SEI found previously, one would expect a Na^+-conducting SEI to be less stable simply due to the higher solubility of NaF (>40 mg per 1 mL at 25 °C) than LiF (<1.34 mg per 1 mL at 25 °C) in water. Fortunately, the dissolution of NaF by water seems to be significantly suppressed by the modest concentration of NaOTF, as shown in Figure 2b. The lower NaF solubility in the "water-in-salt" electrolyte by

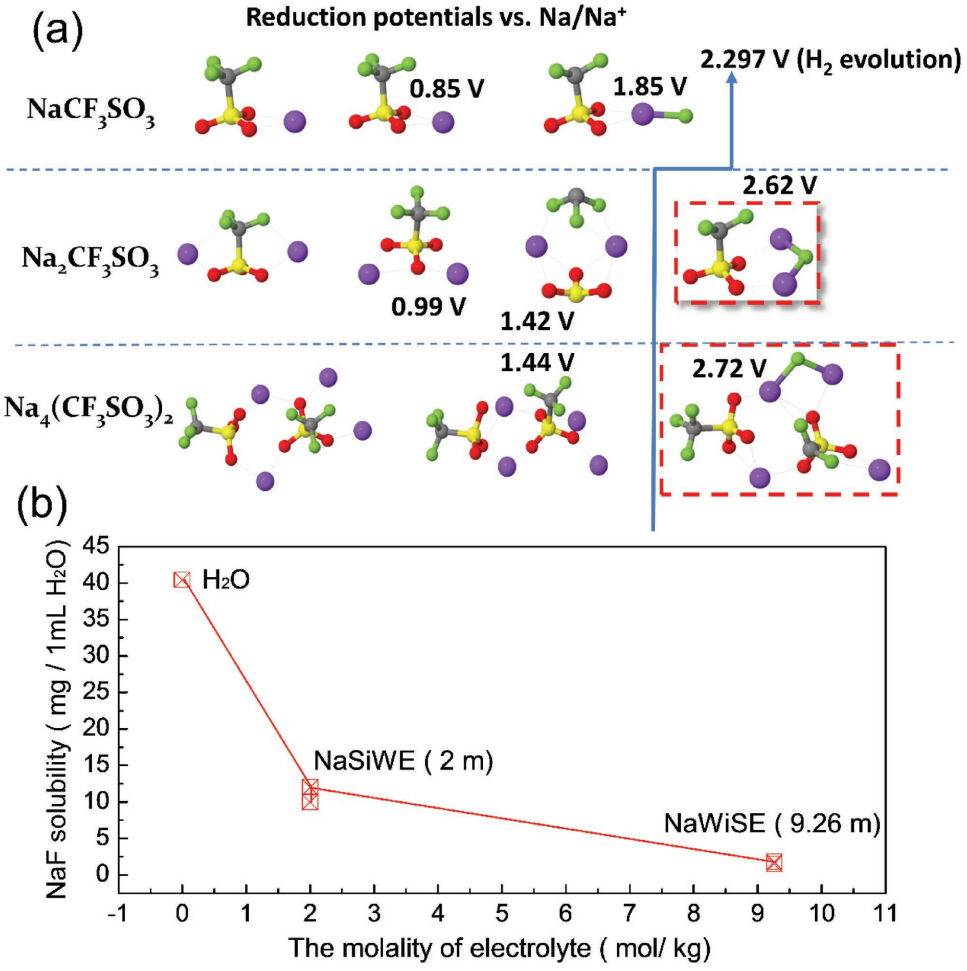

Figure 2. a) Reduction potential of NaOTF complexes from QC calculations using G4MP2 method and SMD (water) implicit solvent model and b) the dependence of NaF solubility in NaTOf–H2O system on salt concentration.

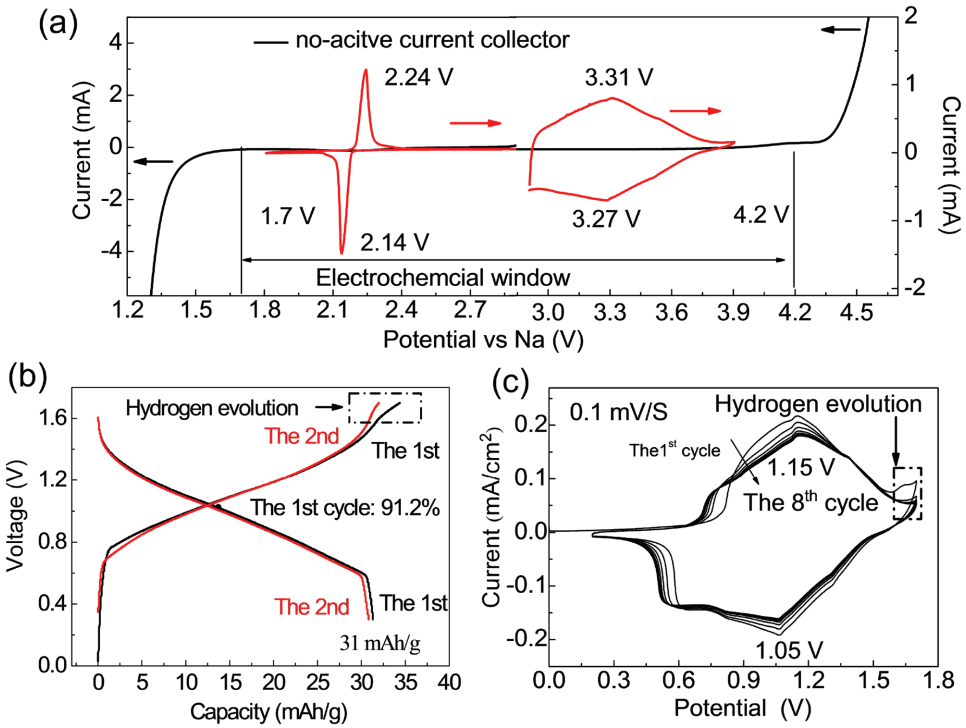

Figure 3. Electrochemical stability of sodium water-in-salt electrolyte (9.26 m NaOTF in H_2O) as evaluated via cycling voltammetry (CV) and galvanostatic charge/discharge experiments on both inert (stainless steel grid) and active working electrodes. a) the CV curves measured on inert electrodes at the scanning rate of 10 mV s^{-1}, which is overlaid with the 1st CV traces obtained on active anode ($NaTi_2(PO_4)_3$) and cathode ($Na_{0.66}[Mn_{0.66}Ti_{0.34}]O_2$) materials at the scanning rate of 0.1 mV s^{-1}, b,c) the repeated galvanostatic (obtained at 0.2 C rate) and cyclic voltammetric (obtained at scanning rate of 0.1 mV s^{-1}) cyclings of $Na_{0.66}[Mn_{0.66}Ti_{0.34}]O_2/NaTi_2(PO_4)_3$ full Na-ion cell. The hydrogen evolution in full cell can be visualized by the difference between the initial and the following cycles when the SEI has been stabilized.

more than 10 times as compared with neat water should ensure sufficient stability of the NaF-based SEI against electrolyte dissolution.

Cycling voltammetry (CV) was used to evaluate the electrochemical stability window of NaWiSE on inert stainless steel electrodes using (**Figure 3**a), as well as sodiation/desodiation behaviors of $NaTi_2(PO_4)_3$ anode, $Na_{0.66}[Mn_{0.66}Ti_{0.34}]O_2$ cathode (inset in Figure 3a), and the corresponding $NaTi_2(PO_4)_3$/$Na_{0.66}[Mn_{0.66}Ti_{0.34}]O_2$ full cell in NaWiSE (Figure 3c). The overall NaWiSE window is nearly 2.5 V as shown in Figure 3a, with cathodic and anodic limits located at 1.7 and 4.2 V versus Na, respectively. As demonstrated in Figure 3a, this window should be wide enough to envelop the electrochemical couple of $Na_{0.66}[Mn_{0.66}Ti_{0.34}]O_2$ and $NaTi_2(PO_4)_3$. It is known that CV at fast scan rates tends to overestimate electrochemical stability window, where the onset currents of various parasitic reactions could be kinetically hidden. Using a slower scan rate (0.1 mV s^{-1}), which would more closely simulate what electrolyte experiences in an actual $Na_{0.66}[Mn_{0.66}Ti_{0.34}]O_2$/$NaTi_2(PO_4)_3$ battery, an irreversible process is hence revealed to occur above 1.6 V during the first charging (Figure 3c). This process could be attributed to both SEI formation (OTF-anion reduction) and simultaneous breaking down of water (hydrogen evolution) at the $NaTi_2(PO_4)_3$ anode surface. The separate galvanostatic cyclings of $NaTi_2(PO_4)_3$ anode and $Na_{0.66}[Mn_{0.66}Ti_{0.34}]O_2$ cathode (Figure S12, Supporting Information) obtained in a three-electrode cell configuration and the corresponding $Na_{0.66}[Mn_{0.66}Ti_{0.34}]O_2/NaTi_2(PO_4)_3$ full cell in the first two cycles were also evaluated in NaWiSE (Figure 3b). After the initial cycles, the irreversible processes apparently diminish and eventually disappear, which is a typical behavior of SEI formation and subsequently stabilization (Figure 3c). The pristine morphologies of both $NaTi_2(PO_4)_3$ anode and $Na_{0.66}[Mn_{0.66}Ti_{0.34}]O_2$ cathode were examined under scanning electron microscope (SEM) and transmission electron microscopy (TEM), as presented in Figures S13 and S14 (Supporting Information), respectively.

The galvanostatic charge/discharge performances of $Na_{0.66}[Mn_{0.66}Ti_{0.34}]O_2/NaTi_2(PO_4)_3$ full cells were evaluated in three different Na electrolytes with the varying salt concentrations: 2 m $NaCF_3SO_3$ ("salt-in-water" electrolyte, or NaSiWE), 9.26 m $NaCF_3SO_3$ (NaWiSE), and 1 m Na_2SO_4 (**Figure 4** and Figure S15 (Supporting Information)). In order to compensate for the Na consumption due to the SEI formation and subsequent stabilization process, the excess cathode was used against the anode at a mass ratio of 2:1, which translates to an excess of ≈5% molar Na at the cathode side on the basis of the reported reversible capacities (≈70 mA h g^{-1}) of $Na_{0.66}[Mn_{0.66}Ti_{0.34}]O_2$[3] and the theoretical capacities (133 mA h g^{-1}) of $NaTi_2(PO_4)_3$. In NaWiSE electrolytes, the full cells demonstrated an average voltage of 1.0 V and discharge capacity of 31 mA h g^{-1} based on the total electrode mass at 0.2 C, which translates into individual cathode and anode capacities of 62 and 93 mA h g^{-1}, respectively (Figure 3b). An energy density of 31 W h kg^{-1} was

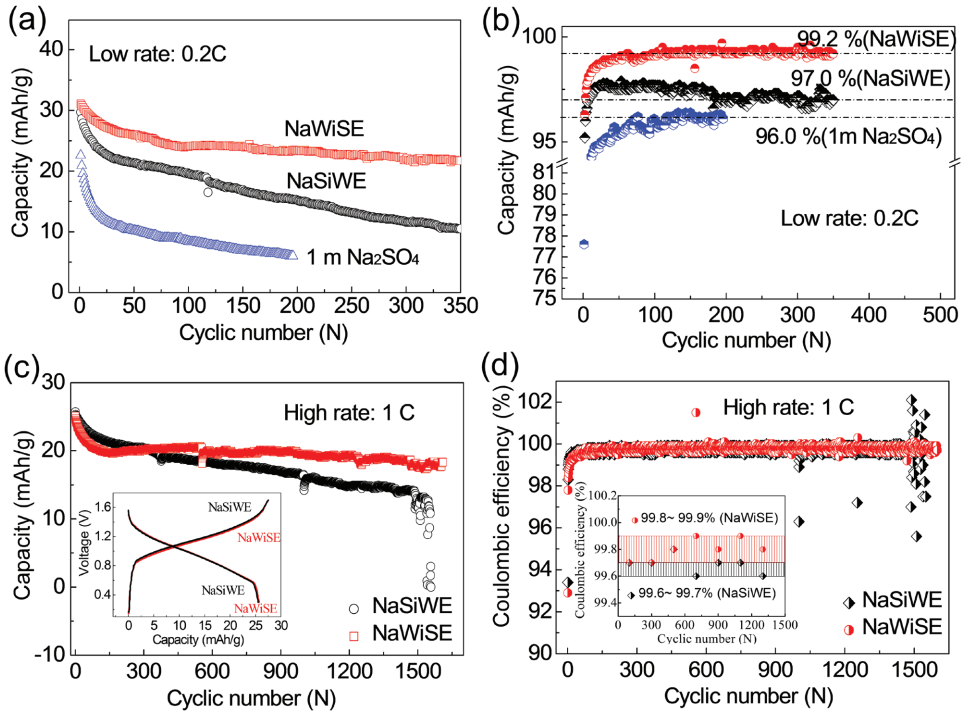

Figure 4. Electrochemical performances of $Na_{0.66}[Mn_{0.66}Ti_{0.34}]O_2/NaTi_2(PO_4)_3$ full cell in different aqueous electrolytes (NaSiWE: 2 m $NaCF_3SO_3$, NaWiSE: 9.26 m $NaCF_3SO_3$ and 1 m Na_2SO_4). a,b) Cycle life and the Coulombic efficiency at low rate (0.2 C); c,d) at high rate (1 C) with the corresponding initial voltage profiles presented in inset. The cells were cycled within voltage range of 0.3 to 1.7 V, and the cathode–anode mass ratio is set at 2:1 by weight.

thus delivered based on the total electrode mass. Judging from the materials used in the cell configuration (70% active materials including cathode and anode; 30% nonactive materials including separator, electrolyte and current collector, and so on), we roughly estimated that the energy density of our proposed system should be above 20 W h kg^{-1} at cell level. Since Na source is limited in full cell, Coulombic efficiency is the critical factor determining not only how long the cell would survive but also how reversible the electrochemistry is. As Figure 4b shows, the Coulombic efficiencies of such Na-ion full cells enabled by 1 m Na_2SO_4, NaSiWE, and NaWiSE are 77.6%, 88.2%, and 91.2% in the first cycle (Figure 3b and Figure S15 (Supporting Information)), respectively, which gradually increase in the following cycles and ultimately stabilize at 96.0% (1 m Na_2SO_4), 97.0% (NaSiWE), and 99.2% (NaWiSE), respectively. As expected, much better cyclic cycling stability and lower capacity fading rate (0.086% per cycle) were achieved in NaWiSE than 1 m Na_2SO_4 (0.37% per cycle) and NaSiWE (<0.18% per cycle). The suppression of water decomposition by formation of SEI is apparently responsible for the superior performances of the Na-ion full cell in NaWiSE.

It should be noted that Coulombic efficiency depends on the charge–discharge rate. At a high rate of 1 C, there is a little difference between the Coulombic efficiencies of NaSiWE (99.7%) and NaWiSE (99.9%), a result of hydrogen evolution as a parasitic process being less competitive at such high rate against electrochemical sodiation/desodiation reactions in both electrolytes. However, such "pseudostability" of NaSiWE due to kinetic hindrance of parasitic reaction is not of practical significance, as in actual applications, the capacity has to be gained at slow rates and also be retained at charged states during long-term standing. Upon closer examination, since sodiation potential of $NaTi_2(PO_4)_3$ (2.1 V vs Na) is slightly lower than that of hydrogen evolution in neutral aqueous NaSiWE (2.29 V vs Na), simultaneous hydrogen evolution inevitably occurs in all previously reported aqueous Na-ion batteries.[6] Thus, the high Coulombic efficiencies reported in previous literature with diluted electrolytes are the result of such pseudostability. As taught by Dahn and coworkers, cycle life and reversibility of batteries obtained at high rates do not reflect stable operation in real battery environments.[20] Only in the presence of an aqueous SEI formed in NaWiSE can superior cycling performance and Coulombic efficiency >99% be maintained at low rate of 0.2 C (Figure 4). This improvement removes a major barrier to the practical application of aqueous Na-ion batteries.

To confirm that an aqueous SEI has been formed in NaWiSE, high resolution TEM images of $NaTi_2(PO_4)_3$ anode before and after cycles were collected as direct evidences (**Figure 5**). On pristine surface of nanosized $NaTi_2(PO_4)_3$ anode only a thin carbon coating can be observed (Figure 5a,b); however, after prolonged cycling (1000 cycles at 1 C), an extra layer of partially crystalline species with the thickness of 4–6 nm was detected (Figure 5d), which uniformly covers the surface. The interplanar space of this new layer was found to be in the range of 0.25–0.26 nm, almost identical to the perfect crystalline NaF (0.234 nm (200)) (Figure 5c). It should also be noted that, even in NaSiWE, the presence of SEI can still be detected on the anode particle after 1000 cycles, with the only difference

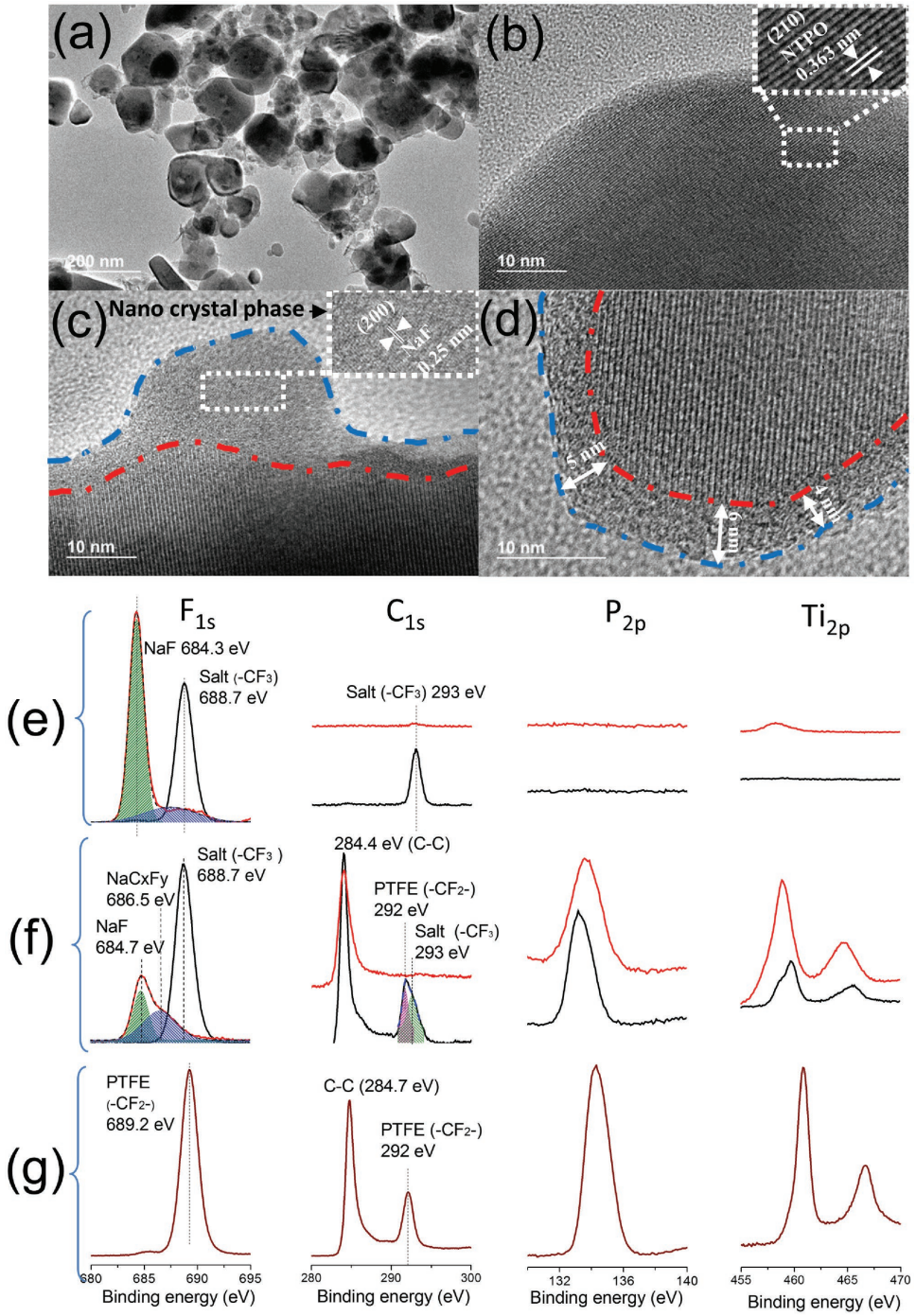

Figure 5. SEI on the $NaTi_2(PO_4)_3$ anode. a,b) TEM images of $NaTi_2(PO_4)_3$ particle before and after galavanostatic cycling. (a) Pristine $NaTi_2(PO_4)_3$ and its high-resolution image (b), c) high-resolution images of $NaTi_2(PO_4)_3$ after cycling in NaWiSE for 421 times at 0.2 C, and d) after 1000 cycles at 1 C. e,f) XPS spectra of $NaTi_2(PO_4)_3$ electrodes before and after cycled. (e) After 1 cycle in NaWiSE; (f) after 1 cycle in NaSiWE electrolyte. The black and red solid lines represent the cycled electrodes without sputtering and with Ar ion sputtering for 15 min, respectively. g) The pristine electrode.

being that the SEI in this case is not as robust as that formed in NaWiSE (Figure S16, Supporting Information). However, it still exerts certain effect on the suppression of electrolyte decomposition as compared to the Na_2SO_4 electrolyte, which does not form any SEI on anode surface, as evidenced by the performance difference in Figure 4a,b.

X-ray photoelectron spectroscopy (XPS) with Ar-ion sputtering was performed on the cycled electrode (Figure 5e,f) and the pristine electrode (Figure 5g), which revealed clear NaF presence on anode surface after cycling in both NaWiSE and NaSiWE. Adopting F 1s signal from the salt as a relative reference for comparison, it becomes immediately obvious that the

intensity of NaF from NaWiSE is significantly higher than that from NaSiWE. More interestingly, in sharp contrast with the electrode cycled in NaSiWE, which yielded signals of C, P, and Ti corresponding to poly(vinylidene difluoride) (PTFE) binder ($-CF_2-$), carbon additive and active material (P and Ti), respectively, the electrode recovered from NaWiSE did not yield any of those signals, even after prolonged (15 min) sputtering was applied in order to remove any possible residual salt on its surface. Therefore, the NaF-based SEI formed by NaWiSE on the anode must be extremely dense and robust, which completely shielded all the elements contained by the electrode composite.

If the NaF-based SEI cannot insulate electron tunneling, side chemical reaction between electrolyte and the fully sodiation electrode $Na_{1+x}Ti_2(PO_4)_3$ ($x \leq 2$) is expected to occur spontaneously in open circuit (Equation (1))

$$x\mathrm{H_2O_{(l)}} + \mathrm{Na_{1+x}Ti_2(PO_4)_{3(s)}} \rightarrow x\mathrm{NaOH_{(s)}} + \mathrm{NaTi_2(PO_4)_{3(s)}} + 0.5x\mathrm{H_{2(g)}} \quad (1)$$

resulting in sodium loss at anode and hydrogen build-up. Thus, a real rigorous test of the SEI stability is the long-term storage at 100% state of charge (SOC), which has never been conducted in any reported aqueous Na-ion battery work. As shown by **Figure 6**a,b, such a rigorous self-discharge test is performed with fully sodiated $Na_3Ti_2(PO_4)_3$ anode in aqueous electrolyte by monitoring the decay of its open circuit voltage (OCV). Clearly, it took much longer for the OCV to drop from 1.1 to 0.8 V in NaWiSE (710 h) than in NaSiWE (540 h) (Note: 1.1 V is the potential difference between desodiated $Na_{0.66}[Mn_{0.66}Ti_{0.34}]O_2$ and sodiated $Na_{1+x}Ti_2(PO_4)_3$, and 0.8 V is the potential difference between desodiated $Na_{0.66}[Mn_{0.66}Ti_{0.34}]O_2$ and desodiated $NaTi_2(PO_4)_3$ due to capacity loss by anode via self-discharge). Meanwhile, after 10 h resting at fully charged state (100% SOC), the Coulombic efficiencies were also plotted against cyclic number (Figure 6b) for NaWiSE, which gradually increase and approach 100%, revealing that the formation and continuous perfection of a protective SEI took time. After 500 cycles, the Coulombic efficiency increased from 96.2% to 98.7%, where the hydrogen evolution should have been significantly suppressed. The capacity loss is asymptotical, manifesting that the self-discharge is most severe right after the very first full-charge (100% SOC) and then rapidly tapers off. Using commercial LIB as benchmark, the capacity loss is above 5% in the initial 24 h. Therefore, the Coulombic efficiencies of 96.2% at the 21st cycle

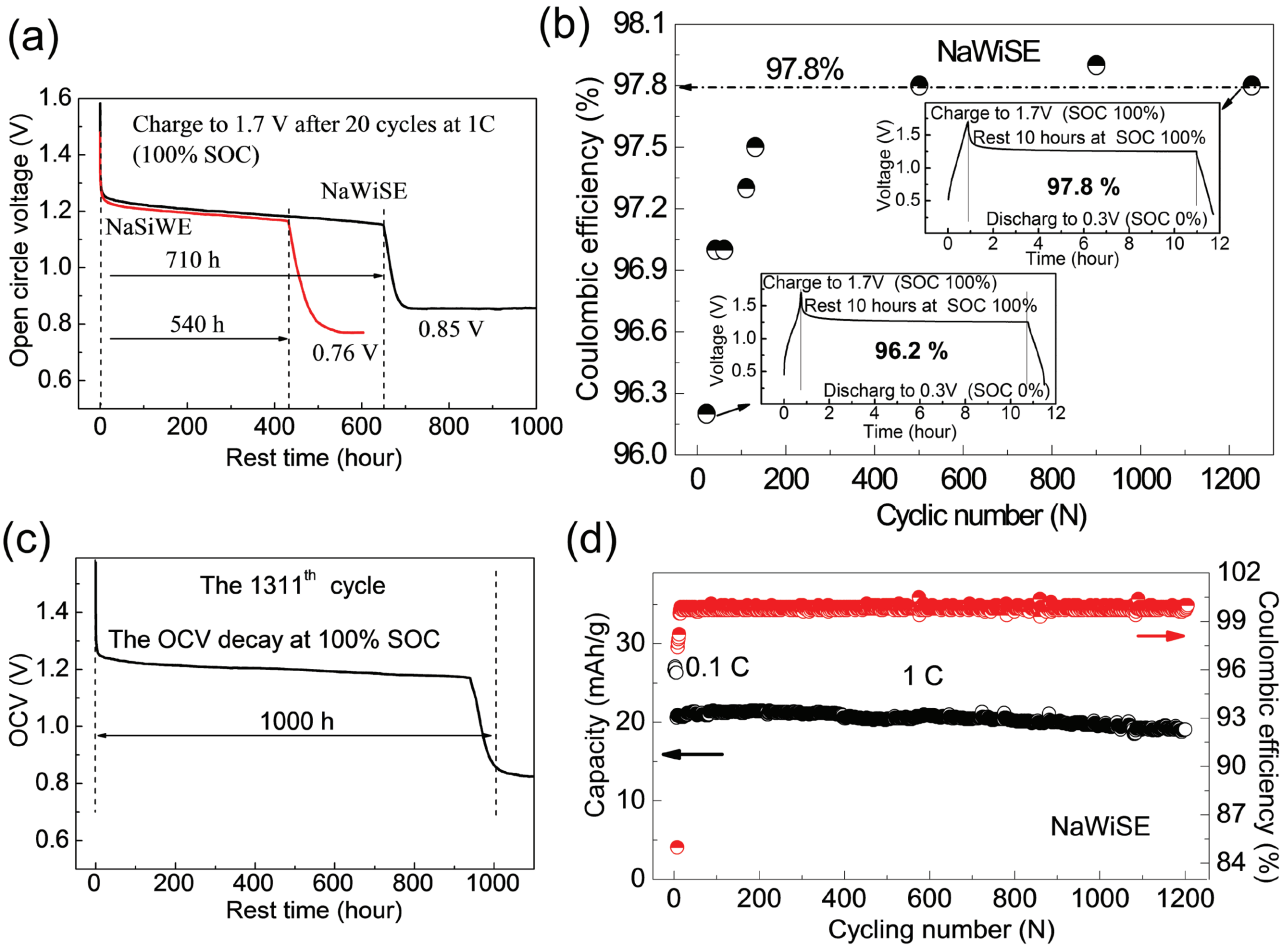

Figure 6. The evaluation of SEI durability in full cell. a) OCV decay at fully charged state (100% SOC) in both NaSiWE and NaWiSE at 1C, and b) Coulombic efficiencies after resting at 100% SOC for 10 h at every several cycles. Inset: the voltage profiles of charging and discharging immediately before and after the 10 h rest. The self-discharge was evaluated by comparison with the columbic efficiency and the capacity loss after resting. c) The OCV decay at 100% SOC after 1311 cycles, and d) the cycle life and Coulombic efficiency at 1 C after initial low-rate cycles.

and of 97.8% represent a low self-discharge rate comparable to the state-of-the-art LIB. Subsequently, at the 1311th cycle where robust SEI is fully formed, the battery is fully charged again to 100% SOC with its OCV decay monitored (Figure 6c). Surprisingly, it took over a whole month (>940 h) for the OCV to drop below 1.0 V. For the self-discharge rate, a general approach is to maintain the cell at different SOC period, then discharge it to calculate the capacity lost during the holding. Here, we assume that OCV decay is the result of the anode capacity loss, and that the OCV dipping under 1.0 V indicates the loss of all sodium-ion in the anode host via self-discharge with a capacity loss of 100%. Thus, based on the recorded cutoff time (940 h), the self-discharge rate should be 100% divided by 940 h, or <0.106% h^{-1}. (Note: 1.1 V is the potential difference between desodiated $Na_{0.66}[Mn_{0.66}Ti_{0.34}]O_2$ and sodiated $Na_{1+x}Ti_2(PO_4)_3$, and 0.8 V is the potential difference between desodiated $Na_{0.66}[Mn_{0.66}Ti_{0.34}]O_2$ and desodiated $NaTi_2(PO_4)_3$ due to capacity loss by anode via self-discharge). This stability is unprecedented for any aqueous Li- or Na-ion batteries reported.

Realizing that SEI growth is time dependent,[21] we performed low rate (0.1 C) formation in the initial 5 cycles before subjecting the cell to long-term cycling at higher rate of 1 C. As shown in Figure 6d, the full Na-ion cell with SEI thus formed exhibited excellent reversibility with high capacity retention of 92.7% after 1200 cycles and high Coulombic efficiency of >99.9%. To push for a more extreme condition, we raised the cutoff voltage from 1.7 to 2.0 V, and observed that the cell with NaWiSE still showed excellent cycling stability (Figure S17, Supporting Information). Compared with NaSiWE, hydrogen evolution NaWiSE seemed to be negligible, only occurring during the initial cycles and diminishing rapidly, as indicated by the high Coulombic efficiency of 99% after just 20 cycles.

All the results shown above convincingly suggest that a durable, dense, and robust Na^+-conducting SEI has been formed in super-concentrated NaWiSE. The presence of this robust SEI casts a significant effect on prolonging cycling life, increasing Columbic efficiency, reducing self-discharge, and improving overcharge performance. This approach thus renders the aqueous Na-ion battery more practical than ever before.

3. Conclusion

In this work, we successfully demonstrated for the first time that a Na^+-conducting SEI can be formed in concentrated sodium version of "water-in-salt" electrolyte. This SEI expands the usable electrochemical window to 2.5 V for a Na-ion battery constructed with $NaTi_2(PO_4)_3$ and $Na_{0.66}[Mn_{0.66}Ti_{0.34}]O_2$. Raman spectra together with molecular scale simulations revealed that cation–anion interaction and occurs much more intensely in Na-ion electrolytes, resulting in pronounced ion aggregation and, more importantly, the intimate Na–F contacts. This factor played a key role in raising the anion reduction potential in order to defeat water decomposition, and enables the formation of a stable and reparable SEI at much lower salt concentration than its Li counterparts. Thanks to the kinetic protection provided by this SEI, parasitic reactions in full Na-ion battery constructed on $NaTi_2(PO_4)_3$ and $Na_{0.66}[Mn_{0.66}Ti_{0.34}]O_2$ were minimized, leading to remarkable capacity retention improvements no matter upon storage at 100% SOC or cycling at low rates. This Na-ion full cell achieved an energy density of 31 W h kg^{-1} with nearly 100% Coulombic efficiency (99.7%) at 0.2 C for >350 cycles, or superior long cycle life >1200 times at 1 C. We anticipate that the introduction of Na^+-conducting aqueous SEI into aqueous Na-ion batteries will open a new pathway for its practical application in electric energy storage systems.

4. Experimental Section

Material Synthesis: Aqueous electrolytes are prepared according to molality (mol-salt in kg-solvent), which were coded by abbreviated concentrations (2, 4, 6, and 9.26 m), respectively. $Na_{0.66}[Mn_{0.66}Ti_{0.34}]O_2$ cathode was prepared by a solid state reaction at 900 °C for 12 h using precursors Na_2CO_3 (99%), Mn_2O_3 (99%), and TiO_2 (99.5%) with the stoichiometric ratio of 1.05:1.00:1.00. Pristine $NaTi_2(PO_4)_3$ anode was synthesized by a sol–gel method. Stoichiometric amounts of $NaNO_3$, $NH_4H_2PO_4$, and citric acid were first dissolved in deionized (DI) water, followed by the addition of a diluted tetrabutoxytitanium solution in ethanol to reach the final stoichiometry under vigorously stirring. Finally, after evaporating the solvent, the gel precursor was annealed at 700 °C for 12 h in air. The carbon-coated $NaTi_2(PO_4)_3$ was prepared by a chemical vapor deposition method at 800 °C for 6 h, which was placed in a quartz tube furnace and a toluene (C_7H_8) vapor was carried by Ar gas.

Material Characterizations: SEM and TEM were examined in a Hitachi S-4700 operating at 10 kV and at a JEOL 2100 F field emission, respectively. Raman spectra were collected with a Horiba Jobin Yvon Labram Aramis using a 532 nm diode-pumped solid-state laser between 1200 and 100 cm^{-1}, with all the samples sealed in a glass test tube. XPS analysis was performed on a high resolution Kratos AXIS 165 X-ray photoelectron spectrometer using monochromic AlKa radiation source. All samples were recovered from full aqueous Na-ion cell in 2032 coin cell configuration after electrochemical cycles. The electrodes were rinsed by DME three times and then dried under vacuum for half an hour before XPS measurement.

Electrochemical Measurements: Ionic conductivity was measured with electrochemical impedance spectroscopy (EIS) with Gamry impedance analyzer. The samples were equilibrated in a temperature chamber over a temperature range of 10 to 50 °C. At each set temperature, the sample was left standing for at least 0.5 h before EIS was collected. The conductivity cell constants were predetermined using 0.01 M aqueous KCl standard solution at 25 °C. Composite electrodes were fabricated by compressing active materials, carbon black, and PTFE at weight ratio of 8:1:1 on a stainless steel grid. The full aqueous Na-ion cell was assembled in CR2032-type coin cell, which were cycled galvanostatically on a Land BT2000 battery test system (Wuhan, China) at room temperature (28–30 °C).

Supporting Information

Supporting Information is available from the Wiley Online Library or from the author.

Acknowledgements

This work was supported by the DOE ARPA-E (DEAR0000389). The authors also acknowledge the support of the National Key R&D Program of China (No. 2016YFB0901500) and the NSFC (51421002).

Conflict of Interest

The authors declare no conflict of interest.

Keywords

aqueous sodium-ion electrolyte, aqueous sodium-ion batteries, high concentrated electrolyte, sodium-ion batteries, water-in-salt

Received: May 1, 2017
Revised: May 22, 2017
Published online: July 21, 2017

[1] a) Z. Yang, J. Zhang, M. C. W. Kintner-Meyer, X. Lu, D. Choi, J. P. Lemmon, J. Liu, *Chem. Rev.* **2011**, *111*, 3577; b) V. Palomares, P. Serras, I. Villaluenga, K. B. Hueso, J. Carretero-Gonzalez, T. Rojo, *Energy Environ. Sci.* **2012**, *5*, 5884; c) H. Pan, Y.-S. Hu, L. Chen, *Energy Environ. Sci.* **2013**, *6*, 2338; d) B. Dunn, H. Kamath, J.-M. Tarascon, *Science* **2011**, *334*, 928.

[2] C. D. Wessells, S. V. Peddada, R. A. Huggins, Y. Cui, *Nano Lett.* **2011**, *11*, 5421.

[3] Y. Wang, L. Mu, J. Liu, Z. Yang, X. Yu, L. Gu, Y.-S. Hu, H. Li, X.-Q. Yang, L. Chen, X. Huang, *Adv. Energy Mater.* **2015**, *5*, 1501005.

[4] M. Pasta, C. D. Wessells, N. Liu, J. Nelson, M. T. McDowell, R. A. Huggins, M. F. Toney, Y. Cui, *Nat. Commun.* **2014**, *5*, 3007.

[5] a) W. Li, J. R. Dahn, D. S. Wainwright, *Science* **1994**, *264*, 1115; b) J.-Y. Luo, W.-J. Cui, P. He, Y.-Y. Xia, *Nat. Chem.* **2010**, *2*, 760; c) F. Beck, P. Ruetschi, *Electrochim. Acta* **2000**, *45*, 2467.

[6] H. Kim, J. Hong, K. Y. Park, H. Kim, S. W. Kim, K. Kang, *Chem. Rev.* **2014**, *114*, 11788.

[7] a) C. Wessells, R. A. Huggins, Y. Cui, *J. Power Sources* **2011**, *196*, 2884; b) C. Wessells, R. Ruffo, R. A. Huggins, Y. Cui, *Electrochem. Solid-State Lett.* **2010**, *13*, A59.

[8] a) Z. Li, D. Young, K. Xiang, W. C. Carter, Y.-M. Chiang, *Adv. Energy Mater.* **2013**, *3*, 290; b) X.-Y. Wu, M.-Y. Sun, Y.-F. Shen, J.-F. Qian, Y.-L. Cao, X.-P. Ai, H.-X. Yang, *ChemSusChem* **2014**, *7*, 407; c) C. W. Mason, F. Lange, *ECS Electrochem. Lett.* **2015**, *4*, A79; d) Z. Li, D. B. Ravnsbaek, K. Xiang, Y.-M. Chiang, *Electrochem. Commun.* **2014**, *44*, 12; e) Z. Hou, X. Li, J. Liang, Y. Zhu, Y. Qian, *J. Mater. Chem. A* **2015**, *3*, 1400; f) B. Zhao, Q. Wang, S. Zhang, C. Deng, *J. Mater. Chem. A* **2015**, *3*, 12089; g) S. Il Park, I. Gocheva, S. Okada, J.-I. Yamaki, *J. Electrochem. Soc.* **2011**, *158*, A1067; h) X. Li, X. Zhu, J. Liang, Z. Hou, Y. Wang, N. Lin, Y. Zhu, Y. Qian, *J. Electrochem. Soc.* **2014**, *161*, A1181; i) W. Wu, S. Shabhag, J. Chang, A. Rutt, J. F. Whitacre, *J. Electrochem. Soc.* **2015**, *162*, A803.

[9] Q. T. Qu, L. L. Liu, Y. P. Wu, R. Holze, *Electrochim. Acta* **2013**, *96*, 8.

[10] C. Deng, S. Zhang, Z. Dong, Y. Shang, *Nano Energy* **2014**, *4*, 49.

[11] D. J. Kim, Y. H. Jung, K. K. Bharathi, S. H. Je, D. K. Kim, A. Coskun, J. W. Choi, *Adv. Energy Mater.* **2014**, *4*, 1400133.

[12] a) H. Qin, Z. P. Song, H. Zhan, Y. H. Zhou, *J. Power Sources* **2014**, *249*, 367; b) L. Chen, W. Li, Y. Wang, C. Wang, Y. Xia, *RSC Adv.* **2014**, *4*, 25369; c) X. Dong, L. Chen, J. Liu, S. Haller, Y. Wang, Y. Xia, *Sci. Adv.* **2016**, *2*, e1501038.

[13] Y. Liu, B. H. Zhang, S. Y. Xiao, L. L. Liu, Z. B. Wen, Y. P. Wu, *Electrochim. Acta* **2014**, *116*, 512.

[14] L. Suo, O. Borodin, T. Gao, M. Olguin, J. Ho, X. Fan, C. Luo, C. Wang, K. Xu, *Science* **2015**, *350*, 938.

[15] A. V. Cresce, M. Gobet, O. Borodin, J. Peng, S. M. Russell, E. Wikner, A. Fu, L. B. Hu, H. S. Lee, Z. C. Zhang, X. Q. Yang, S. Greenbaum, K. Amine, K. Xu, *J. Phys. Chem. C* **2015**, *119*, 27255.

[16] Y. Marcus, *Chem. Rev.* **2009**, *109*, 1346.

[17] K. Xu, *Chem. Rev.* **2004**, *104*, 4303.

[18] Y. Yamada, K. Usui, K. Sodeyama, S. Ko, Y. Tateyama, A. Yamada, *Nat. Energy* **2016**, *1*, 16129.

[19] a) L. Suo, O. Borodin, W. Sun, X. Fan, C. Yang, F. Wang, T. Gao, Z. Ma, M. Schroeder, A. von Cresce, S. M. Russell, M. Armand, A. Angell, K. Xu, C. Wang, *Angew. Chem., Int. Ed.* **2016**, *128*, 7252; b) L. Suo, F. Han, X. Fan, H. Liu, K. Xu, C. Wang, *J. Mater. Chem. A* **2016**, *4*, 6639.

[20] A. J. Smith, J. C. Burns, X. M. Zhao, D. J. Xiong, J. R. Dahn, *J. Electrochem. Soc.* **2011**, *158*, A447.

[21] a) B. Gyenes, D. A. Stevens, V. L. Chevrier, J. R. Dahn, *J. Electrochem. Soc.* **2015**, *162*, A278; b) A. J. Smith, J. C. Burns, S. Trussler, J. R. Dahn, *J. Electrochem. Soc.* **2010**, *157*, A196.

